Journal of New Materials for Electrochemical Systems 5, 203-212 (2002)

Novel Electrochromic Batteries: I. A PB-WO_3 Cell with a Theoretical Voltage of 1.35V

Lin-Chi Chen, Yu-Hsien Huang, Kuei-Sheng Tseng, and Kuo-Chuan Ho*

Department of Chemical Engineering
National Taiwan University
Taipei 10617, Taiwan

(Received June 21, 2001 ; received in revised form January 3, 2002)

Abstract: *Upon considering the fact that the WO_3/H_xWO_3 has a much more negative formal potential than that of the Berlin green (BG)/Prussian blue (PB) redox system, a novel thin-film electrochromic battery (ECB) based on PB and WO_3, designated as PWECB, was proposed and investigated. By using the KCl-saturated poly-2-acrylamido-2-methylpropane sulfonic acid (K-PAMPS) electrolyte that accommodates the conduction of both K^+ and H^+, a PWECB can be charged/discharged reversibly between 0.80 V and 1.80 V and has a theoretical voltage of 1.35 V, which is almost twice the voltage of non-lithium PB-based batteries reported in literature. In addition, the PWECB showed green (charged state)-to-blue (discharged state) electrochromism; therefore, its state of charge (SOC) can be visualized. Visualization of the SOC, by the naked eye, can help people to judge a cell's charging condition. Moreover, it was demonstrated that the ECB with an energy capacity of 37.8 mW-s/cm^2 could drive an 8-digit electronic calculator for several hours. By combining the ECB with a photovoltaic cell (PV), it is possible to realize the all-solar-driven electronic device. Consequently, the combinative PV-ECB power system offers an opportunity to reduce the use of primary button cells, which are disadvantageous to the environment. In addition to these superior applications, the dynamic and at-rest stabilities of the PWECB are discussed in this paper.*

Key words : All-solar-driven, electrochromic battery (ECB), KCl-saturated poly-2-acrylamido-2-methylpropane sulfonic acid (K-PAMPS), Prussian blue (PB), tungsten oxide (WO_3).

1. INTRODUCTION

An electroactive species is considered to be electrochromic (EC) [1] if it changes color in response to a change in its redox state. In recent years, various optical applications of EC materials have been investigated, such as displays [2-3], antiglare mirrors [4], solar-attenuated windows (known as "smart windows"), [5] and photo-imaging devices [6-7]. In this paper, a novel EC application – a secondary thin-film battery with visualization of the state of charge (SOC), the so-called electrochromic battery (ECB), is described. A complementary EC device (ECD) consisting of two EC thin-film electrodes and an electrolyte, by its very nature, has a cell configuration identical to that of a secondary battery. It can reversibly be cycled several thousand times (over 20,000 cycles [8-9]) and exhibits different colors depending upon the corresponding voltages. Therefore, such an ECD not only acts as a rechargeable battery but also offers visualization of the SOC, which helps in judging the residual charge of a battery by the naked eye. However, when compared with commercial batteries, ECDs usually have a much lower theoretical voltage (*ca.* 0.5~0.6 V) and a much smaller coulometric capacity (5 ~30 mC/cm^2) for energy saving and optical attenuation considerations. As a result, an ordinary ECD has never been used to provide DC power and cannot be viewed as a realistic battery.

*To whom correspondence should be addressed: Fax: +886-2-2362-3040; Tel: +886-2-2366-0739; Email: kcho@ms.cc.ntu.edu.tw

With regard to the use of EC electrodes for secondary-battery applications, Prussian blue (PB, iron (III) hexacyanoferrate (II)) [10-11], which is characterized by a polyelectrochromic property and exhibits four corresponding redox states, has been investigated intensively [12-21]. From the most reduced to the most oxidized, the four redox states of PB are the colorless Everitt's salt (ES), PB, Berlin green (BG), and Prussian yellow (PY). Except for PY, all redox states can reversibly be formed in a K^+-containing electrolyte [10-11]. By observing that the formal potentials for the PB/ES and BG/PB redox couples in 1N K_2SO_4 are 0.195V and 0.870V *vs.* SCE, respectively, Neff first reported a secondary battery assembled of two identical PB/graphite electrodes with a theoretical voltage (V°) of 0.68V and a theoretical energy density of 95 mWh/cm^3 [12]. In this PB-PB battery, the positive PB electrode underwent the BG/PB redox reaction; the negative PB electrode accompanied the PB/ES reaction. Although a well sealed, purged PB-PB battery with a cell capacity of 30 mAh could reach a constant voltage of 0.93V for 10 days, a capacity loss of *ca.* 5% per charge-discharge cycle was observed when cycling in 1N $K_2SO_{4(aq)}$. Subsequently, Honda *et al.* [13-14] and Kaneko *et al.* [15] described a solid-state thin-film battery: ITO/PB/Nafion®/PB/ITO. They observed that the use of Nafion®, a solid polymer electrolyte (SPE), could greatly improve the cycle life of a PB-PB cell. In this case, the discharge-to-charge efficiency was kept at 100% for at least 100 cycles. Similarly, Jayalakshmi *et al.* [16] reported a PB/Nafion®/PB cell with a large capacity using the PB/graphite paste electrode, but using non-transparent black graphite paste would block the PB's EC nature. The same shading problem will occur when using graphite substrate [12]. Consequently, only the thin-film ITO/PB/Nafion®/PB/ITO cell [13-15] can act as an ECB. However, the theoretical voltage of a PB-PB battery is too low to have a promising application. Likewise, other reported PB-based batteries, such as the Cu-PB cells [17-18] (V° = 0.38 ~0.47 V) and Prussian blue analogue (PBA)-PB cells (V° = 0.50 V ~0.60V) [19-20], have been found to have the same problem, except for the PB-Li battery. Imanish *et al.* [21] recently investigated the use of PB as the positive electrode in a lithium battery, which would have a theoretical voltage of *ca.* 3.0 V. Nonetheless, it was pointed out that the discharge capacity is very sensitive to the water content inside the PB lattice, and a 30% capacity fading after cycling 10 times was observed. Moreover, Li metal is unstable in practice [22], and graphite, one of the best Li anodes, is not suitable for electrochromic purposes. Therefore, more work is still required in developing an ECB based on the Li/Li$^+$ redox system.

By realizing that the cathodically colored WO_3 [23-25] has a much more negative formal potential than that of the BG/PB redox couple, a novel ECB based on PB and WO_3, namely PB-WO_3 ECB (PWECB), is proposed and studied in this paper. In combination with the KCl-saturated poly-2-acrylamido-2-methylpropane sulfonic acid (PAMPS) [26-27] denoted as K-PAMPS, a new SPE to provide dual ionic conductivity of H^+ and K^+, a PWECB with a theoretical voltage of 1.35V, which is higher than that of a commercial Ni-metal hydride battery, has been attained. Note that the PWECB is different from an ordinary complementary PB-WO_3 ECD [8-9, 28-30], which undergoes the PB/ES redox reaction and only offers a theoretical voltage of *ca.* 0.5V. Additionally, a PWECB exhibits blue-to-dark green electrochromism in response to the discharge-to-charge transition and thus achieves the visualization of the SOC. In this paper, it will be demonstrated that a thin-film PWECB is applicable for low-power electronic devices. Moreover, it will be shown that by combining an ECB with a photovoltaic cell (PV), one can achieve the goal of all-solar-driven consumer electronics. Besides these applications, the cycle life and self-discharging behavior of a PWECB will also be discussed thoroughly.

2. EXPERIMENTAL

All chemicals used in this work were ACS reagent grade and were not further purified prior to use. Deionized water (DIW) with a resistivity of 18.2 MΩ-cm was used throughout. All electrochemical experiments were carried out at room temperature. The detailed experimental conditions are described as follows.

2.1 Preparation of electrochromic thin films

Optically transparent F-doped SnO_2-coated (FTO) glass substrates (Sinonar, T_{550nm} = 80%, R_{sh} = 20 Ω/sq.) with dimensions of 5.0×2.5×0.2 cm^3 were ultrasonically cleaned with 0.1 N HCl for 5 min and then rinsed with DIW. Afterward, a piece of Cu tape (3M Company, 2.5×0.5 cm^2) was applied to one side of the FTO-coated surface as the bus bar, and insulating tapes were applied to maintain an electrode area of 3.0×1.5 cm^2 for each substrate.

The PB film was galvanostatically deposited onto a FTO glass substrate in a plating solution consisting of 10 mM $FeCl_3$, 10 mM $K_3Fe(CN)_6$, 0.1 N KCl, and 1 N HCl. The K^+-rich environment in the plating solution was adopted with the intention of forming the "soluble" PB, $KFe[Fe(CN)_6]$ [11]. While plating, a cathodic current of 20μA/cm^2 was applied to the FTO glass substrate for 34 minutes. After electrodeposition, the as-grown PB film was washed with DIW and then dried in air for at least 24 hours prior to use.

The WO_3 film was potentiostatically deposited onto another FTO glass substrate. The deposition solution was composed of 36.7 vol% peroxy-tungsten acid (PTA) solution, red 30.3 vol% DIW, and 33.0 vol% isopropanol. The PTA solution was prepared by dissolving 1.5 g tungsten powder into a mixture of 30 ml H_2O_2 (30%) and 30 ml DIW, which was modified from [31-34]. Since the dissolution process was highly exothermic, it was carried out in an ice bath at first. After the exothermic reaction was reduced, the solution was placed in air at room

temperature for 24 hours to complete the dissolution. Then a platinum-black coated Pt foil was immersed into the PTA solution for another 20 hours to decompose the excess H_2O_2. Finally, the filtrated PTA solution was employed. During WO_3 deposition, a constant potential of -0.40 V *vs.* SCE was applied to the FTO substrate for 15 min. The as-grown WO_3 films were washed with DIW and then fired at 100°C for 1 hour before use. The WO_3 films such prepared were shown to be lack of crystallinity. It is worthwhile mentioning that a post-heated electrodeposited WO_3 film shows a typical single redox wave in its cyclic voltammogram (see Fig. 2 and refs. [31-32]). In comparison, a non-heated electrodeposited WO_3 film exhibits two separate redox features (see refs. [33-34]), presumably due to the presence of the residual peroxo groups. Therefore, the heat-treated WO_3 film was adopted in this work.

2.2 Preparation of polymer electrolytes and cell assembly

The K-PAMPS electrolyte was obtained by UV polymerization. A KCl-free AMPS monomer solution was first prepared, composed of 47.61 wt% 2-acrylamido-2-methylpropane sulfonic acid (AMPS), 50.65 wt% DIW, 1.69 wt% tetra-(ethylene glycol) diacrylate (TEGDA), and 0.05 wt% bezoin methyl ether (BME), where AMPS, DIW, TEGDA, and BME were the monomer, solvent, cross-linking agent, and initiator, respectively. Before polymerizing, an AMPS monomer solution was saturated with KCl (*Note* : Other K^+-containing salts may also be used, but chloride ions help to achieve a pseudo Ag/AgCl reference-electrode system. See Sec. 2.3). Then UV irradiation (Spectroline, SB-125) with a light intensity of *ca.* 675 $\mu W/cm^2$ was exerted on the KCl-saturated monomer solution (*ca.* 1.10 ml) located in a casting mold (inner volume = $3.0\times1.5\times0.2$ cm^3) for 3 minutes to form a K-PAMPS film. Additionally, PAMPS films were prepared in the same manner, using a KCl-free AMPS solution, for comparison with K-PAMPS films.

For cell assembly, an as-prepared PB and post-heated WO_3 electrodes were used as the positive and negative electrodes, respectively, and a fresh K-PAMPS film was sandwiched between these two EC electrodes to form a laminated PWECB. The assembly was carried out in air and is schematically illustrated in Fig. 1. Unlike in an ordinary complementary PB-WO_3 ECD, WO_3 was not prepolarized (precolored) to H_xWO_3 in advance. After assembling, the PWECB with an active area of 3.0×1.5 cm^2 was sealed with the Torr Seal® cement (Varian, MA, USA).

2.3 Characterizations of the EC electrodes, K-PAMPS electrolyte, and PWECB

The PB and WO_3 films were electrochemically characterized in K-PAMPS electrolytes, using the three-electrode cyclic voltammetry. The voltammetry was performed with a potentiostat/galvanostat (ECO-Chemie, Autolab, PGSTAT30); silver wire and platinum plate were used as the pseudo-reference and auxiliary electrodes, respectively. Since the polymer electrolyte was saturated with KCl, the redox potential of the pseudo-reference electrode was assumed to have a value identical to the redox potential of Ag/AgCl in saturated KCl. The thickness of the EC film was measured by a profile meter (Tencor, Alpha step-200). Additionally, impedance spectroscopy was performed, with the same potentiostat/galvanostat, to compare the ionic conductivity of the K-PAMPS electrolyte with that of the PAMPS electrolyte. When performing the impedance spectroscopy, polymer samples with dimensions of $1.0\times1.0\times0.2$ cm^3 were used and sandwiched in between two platinum plates (1.0×1.0 cm^2). Also, the water content in PAMPS (without KCl) was determined by the difference in weight, before and after drying at 110 °C for 2 hours, from which the molar ratio of H_2O to AMPS was estimated to be *ca.* 7.2.

PWECBs were electrochemically characterized by the two-electrode methods, including cyclic voltammetry and chronopotentiometry. The former was carried out with the potentiostat/galvanostat mentioned above; the latter was performed with a multichannel battery test system (Maccor, Model 2300). When characterizing a PWECB, the cell voltage (PB *vs.* WO_3) was recorded. Besides the electrochemical characterizations, a commercial 8-digit electronic calculator (CASIO, MS-7, 15μW) and a photovoltaic cell (Sinonar, SC-5030, 1.8V/26 mA at 100 mW/cm^2) were used to demonstrate the applicability of the PWECB.

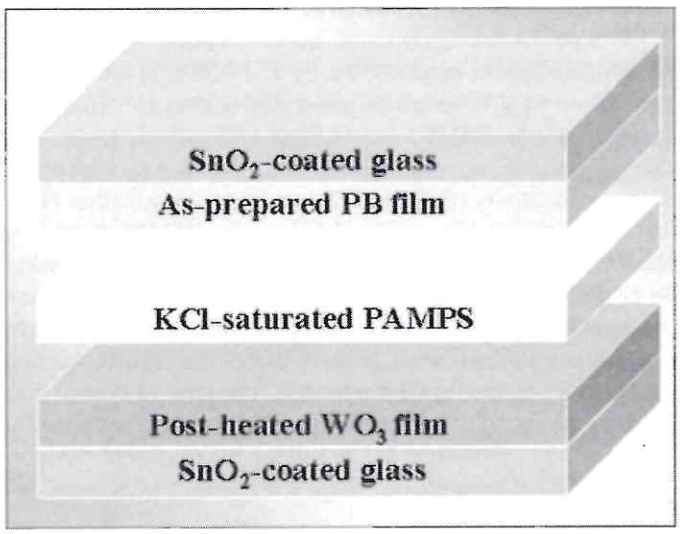

Figure 1: Schematic illustration for assembling a thin-film PWECB.

3. RESULTS AND DISCUSSION

3.1 A PWECB using the K-PAMPS electrolyte and having a theoretical voltage of 1.35 V

3.1.1 The use of the K-PAMPS electrolyte to accommodate the conduction of both K^+ and H^+

In this work, PAMPS [26-27], a well-known H^+ polyelectrolyte, was saturated with KCl to form the K-PAMPS electrolyte to accommodate the conduction of both K^+ and H^+, since K^+ are favored for the electrochromic reaction of PB films [10-11] and H^+ for the reaction of WO_3 films [23-25] due to kinetic reasons. A similar idea was proposed by Habib *et al.*[29], who doped polyvinyl alcohol with H_3PO_4 and KH_2PO_4 to attain a dual ionic conduction of K^+ and H^+ for a complementary PB-WO_3 ECD. Although it was reported that the use of PAMPS in a complementary PB-WO_3 ECD, undergoing the PB/ES and WO_3/H_xWO_3 redox reactions, could achieve a cycle life of more than 20,000 cycles [8], it was observed in this work that K-PAMPS is superior to PAMPS for a PWECB in many respects, including the cell voltage and electrochemical reversibility. Furthermore, it is estimated, according to the concentration ratio of KCl to AMPS in the aqueous monomer solution, that the molar ratio of K^+ to H^+ in a K-PAMPS electrolyte is *ca.* 0.92. This suggests that the amounts of K^+ and H^+ in a K-PAMPS electrolyte are almost equivalent.

The dual conduction of K^+ and H^+ in K-PAMPS has been examined by impedance measurements, which show that the conductivity of a K-PAMPS electrolyte is *ca.* 0.101 S/cm at room temperature, whereas that of a PAMPS electrolyte is *ca.* 0.159 S/cm. As compared with the H^+-conducting PAMPS, a 36.5% decrease in conductivity for K-PAMPS is attributed to the motion of K^+, which migrates slower than H^+ does. It is believed that the PAMPS matrix filled with sulfonic groups acts like the Nafion®, a proton-type cationic exchanging membrane. If the conductivity of K-PAMPS is a linear combination of the intrinsic conductivities of K^+ and H^+ in the PAMPS matrix, the transference numbers for K^+ and H^+ can roughly be estimated to be 18.3% and 81.7%, respectively. In addition, the intrinsic conductivity of K^+ in the PAMPS matrix is estimated to be 0.038 S/cm, which is *ca.* 0.24 times that of the intrinsic conductivity of H^+ in the PAMPS network. The ratio of 0.24 is very close to the mobility ratio of K^+ to H^+ in an aqueous solution, which is 0.21. Therefore, H^+ is still the major charge carrier in a K-PAMPS electrolyte, although the amounts of K^+ and H^+ ions are almost the same.

3.1.2 The BG/PB and WO_3/H_xWO_3 redox systems in a K-PAMPS electrolyte

Prior to describing a PWECB, the EC electrodes used are discussed here. Fig. 2 gives the cyclic voltammograms for an as-prepared PB film with a thickness of *ca.* 1.58 μm and a post-heated WO_3 film with a thickness of *ca.* 0.45 μm in K-PAMPS electrolytes. The corresponding redox couples shown in Fig. 2 are BG/PB and WO_3/H_xWO_3. By taking the average value of the cathodic and anodic peak potentials, the formal potentials of these two redox couples are estimated to be *ca.* 0.974V and *ca.* -0.372V (*vs.* Ag/AgCl/sat'd KCl). In addition, redox capacities of *ca.* 120 mC for BG/PB and *ca.* 146 mC for WO_3/H_xWO_3 (electrode area = 4.5 cm^2) are calculated from Fig. 2. Since the K-PAMPS electrolyte provides both K^+ and H^+, it is generally accepted that PB and WO_3 undergo the following simplified redox reactions [10-11, 23-25]:

$$\text{BG (green)} + 2/3K^+ + 2/3e^- \leftrightarrow \text{PB(blue)} \qquad E_1^o = 0.974\text{V}\textit{vs.}\ \text{Ag/AgCl/sat'd KCl} \quad (1)$$

$$WO_3(\text{colorless}) + x\ H^+ + x\ e^- \leftrightarrow H_xWO_3(\text{blue}) \qquad E_2^o = -0.372\text{V}\textit{vs.}\ \text{Ag/AgCl/sat'd KCl} \quad (2)$$

where $E_1{}^o$ and $E_2{}^o$ are the formal potentials for reactions (1) and (2), respectively. Both redox reactions involve the insertion/extraction of mono-valence cations. The above simplified equations neglect the presence of water in both PB and WO_3 films.

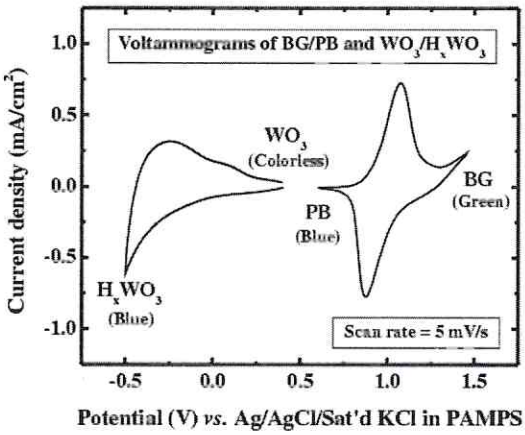

Figure 2: Typical cyclic voltammograms for the BG/PB and WO_3/H_xWO_3 redox couples.

In Eq. (1), the redox mechanism for the "soluble" PB ($KFe[Fe(CN)_6]$) is adopted, because our PB films were prepared in a K^+-rich environment. Furthermore, it was observed experimentally that the BG/PB redox reaction has exactly two-thirds the coulometric capacity of that of the PB/ES redox reaction; it is considered to be a feature of the soluble PB [10-11]. On the other hand, the redox capacity of BG/PB is believed to

possess three-fourths the capacity of that of the PB/ES, a characteristic feature for the "insoluble" PB ($Fe_4[Fe(CN)]_3$) [10]. Hence, BG is here viewed as a solid solution composed of one-third PB ($KFe[Fe(CN)_6]$) and two-thirds PY ($Fe[Fe(CN)_6]$) [10-11], and a theoretical capacity of *ca.* 58.2 mAh/g based on the unit mass of PB is obtained. Moreover, it is thus found that the PB electrodeposition efficiency in the present work is as high as *ca.* 98.2 %. With regard to WO_3, it involves a non-stoichiometric redox reaction (Eq. (2)) and exhibits an asymmetric but reversible voltammogram (Fig. 2). It was reported that the insertion level of H^+ (x in H_xWO_3) could reach a maximum value of 0.5 in $H_2SO_{4(aq)}$ [24]. Recently, Shiyanovskaya *et al.* [34] reported that the x value is not higher than 0.36 for a non-heated electrodeposited WO_3 film. In the present study, the maximum x value of H_xWO_3 corresponding to the CV in Fig. 2 is estimated to be *ca.* 0.33 based on a redox capacity of 32.4 mC/cm^2, a thickness of 0.45 μm, and a density of 5.20 g/cm^3 for the post-heated WO_3 film. The insertion level of 0.33 is close to the critical composition for H_xWO_3, $x_c = 0.32$, at which the nonmetal-to-metal transition occurs [35]. This infers that WO_3 in a K-PAMPS electrolyte showing a more positive electrode potential than -0.5V *vs.* Ag/AgCl/Sat'd KCl is held to be a mixed-valence species [36]. Additionally, x= 0.33 in Eq. (2) indicates a small theoretical capacity of 38.1 mAh/g for WO_3, but a larger theoretical capacity and a more negative formal potential for x > 0.33 can be expected. Although the theoretical capacities for PB and WO_3 are both small as compared with those of commercial batteries, there is no need for adding conductive agents and/or adhesive binders. Besides, the easy preparation, large difference in formal potentials, and EC features look very promising for the applicability of PB and WO_3 to the thin-film battery.

3.1.3 Typical charge/discharge characteristics of a PWECB

According to Eq. (1) and Eq. (2) with $x_{max} = 0.33$ in H_xWO_3, the overall redox reaction of a PWECB is as follows:

$$\begin{aligned} &2WO_3 \text{ (colorless)} + PB \text{ (blue)} + 2/3H^+ \\ &\qquad \text{(The fully discharged state)} \\ &\leftrightarrow 2H_{1/3}WO_3 \text{ (blue)} + \text{BG (green)} + 2/3K^+ \\ &\qquad \text{(The fully charged state)} \end{aligned} \tag{3}$$

Eq. (3) indicates that a PWECB exhibits a blue color corresponding to the fully discharged state and becomes dark green when the PWECB is fully charged. This elucidates that the SOC of a PWECB can be visualized and can be used to judge if a PWECB is workable using the naked eye. This is a superior advantage of an ECB. Furthermore, the theoretical cell voltage of Eq. (3) is calculated to be *ca.* 1.35 V, since the formal potentials for the BG/PB and WO_3/H_xWO_3 redox couples, estimated from Fig. 2, are *ca.* 0.974V and *ca.* -0.372V (*vs.* Ag/AgCl/sat'd KCl), respectively. The theoretical voltage of *ca.* 1.35V is almost twice as high as those of non-lithium PB-based batteries [12-20] and is even higher than that of commercial Ni-MH batteries. This guarantees that a PWECB can function properly without additional cells in series. To verify the theoretical voltage of 1.35 V, the typical charge/discharge curve of a PWECB is given in Fig. 3. It is shown that a PWECB can reversibly be charged/discharged between 0.80V and 1.80V at a rate of 0.2 mA/cm^2(= 0.9 mA, equivalent to a C-rate of *ca.* 26 C). Moreover, the flattest discharge voltage of *ca.* 1.30 V, which is slightly lower than 1.35V, is achieved. The slight difference of 0.05 V is presumably attributed to the high-C discharge and non-unity charge capacity ratio [37] between PB and WO_3, which is avoidable. Besides, since the PWECB is a thin-film battery in nature, it is discharged completely within *ca.* 140 sec at 0.2 mA/cm^2 and thus has a capacity of *ca.* 126 mC. This means that a 4.5-cm^2 thin-film PWECB has an energy capacity of 170 mW-s. Although this value is too small to drive high-power consumer electronics, such as cellular phones and notebook computers, it is capable of driving low-power electronic devices, such as electronic calculators, which take only several μW during operation, for a sufficiently long time. Related demonstrations will be given in the next section.

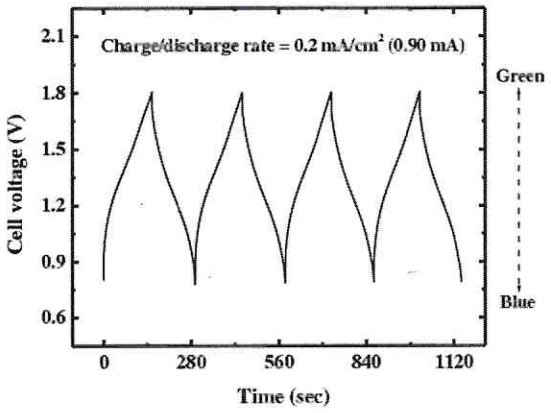

Figure 3: Typical cell voltage for a PWECB charged and discharged at a rate of 0.2 mA/cm^2.

3.2 Applications of the 1.35V PWECB

3.2.1 A secondary battery for the SOC visualization

With regards to battery usage in the real world, a careless random mixing of fresh and exhausted cells will result in a difficulty to distinguish them. However, this problem can be solved when using an ECB, which displays its SOC based on the electrochromism. It is noticed that a PWECB with a cell voltage

of 1.80V is dark green, but the cell becomes truly blue when it arrives at 0.80V. This means that people can judge the cell's residual capacity by directly observing the optical density of the cell. Although various kinds of testers and techniques have been used to monitor the SOC of a "black-box-like" battery, most of them are based on the measurement of the cell voltage, which is not proportional to a battery's charge capacity. Fig. 4 schematically compares the ordinary voltage-monitoring technique and the optical approach for an ECB. It can be seen that with the ordinary technique, it is difficult to achieve a precise prediction of the residual charge, since the Q-V relationship is governed by the Nernst equation and behaves as an S-shaped curve, as shown on the left-hand side of Fig. 4. For instance, a lithium battery, which obeys the Nernst equation and has a theoretical voltage of 3.6 volts, will only show a 3.13% difference in cell voltage at 25°C when the discharging depth goes from 10% to 90%. In comparison, the optical density of an ECB is governed by the Beer law and is proportional to the amount of the residual charge [1], as plotted on the right-hand side of Fig. 4. Thus the optical approach is superior to the conventional voltage method. In practice, a similar optical method has been employed in commercial battery testers, such as Power Check® (Duracell Co.), to reveal the residual charge with an attached color ruler (indicator); however, these SOC-visualized testers are not suitable for simultaneous monitoring because they consume significant amounts of charge while performing the test. Therefore, an ECB, changing color by itself in response to a cell voltage change, has the potential to act as a secondary battery with SOC visualization.

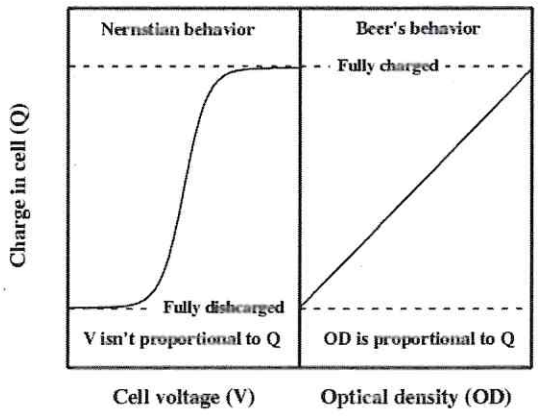

Figure 4: Schematic illustrations of the capacity-monitoring techniques for a battery based on the voltage and optical measurements.

3.2.2 Applications to low-power electronic devices and all-solar-driven devices

Besides the blue-to-dark green electrochromism offering the SOC visualization, it has been demonstrated that a thin-film PWECB having a theoretical voltage of 1.35V and an energy capacity of *ca.* 37.8 mW-s/cm^2 is able to drive low-power electronic devices for a sufficiently long period. Fig. 5 is a demonstration of the PWECB-powered 8-digit electronic calculator (Casio, MS-7) in action. In addition to the calculator, a PWECB-powered electronic timer and electronic temperature-humidity indicator were successfully demonstrated, too. Theoretically speaking, a 4.5-cm^2 PWECB, providing an energy capacity of 170 mW-s, can sustain the operation of the calculator for at least three hours, since it was observed that the maximum power required for operating the calculator is *ca.* 15 μW. In fact, we observed a longer powering duration because the calculator is equipped with a power-managing device, which shuts down the power automatically when the calculator is idle. Of course, if a PWECB with a larger energy capacity is assembled, it will drive a low-power device longer and even provide a chance for use in high-power consumer electronics. By combining a PWECB with a photovoltaic (PV) cell, the goal of an all-solar-driven electronic device has been achieved. To date, there exist only a few solar-powered electronic devices because a device powered by a PV cell may abruptly shut down under poor illumination conditions. Accordingly, most devices equipped with solar cells are two-way powered. In a two-way powered device, a primary button cell is installed as the supplementary or even the main power source. In comparison, an electronic device using the combinative PV-PWECB power system requires no additional, auxiliary button cell. It was demonstrated, as shown in Fig. 6, that the PV cell not only powers the calculator but also charges the PWECB in well-illuminated conditions. When the illumination became poor, the PWECB discharged and sustained the operation of the calculator. Moreover, the color of the PWECB indicated whether the photo-induced charging was needed or not. As a result, the combinative PV-ECB power system fulfills the reality of an all-solar-driven low-power electronic device. This implies that the use of primary button batteries, which are harmful to the environment, can greatly be eliminated when the PV-ECB power system technology matures.

3.3 Dynamic and at-rest stabilities of a PWECB

So far, the principle and applications of a PWECB have been described. To further examine the applicability of a PWECB, the experimental results with respect to the dynamic and at-rest stabilities are presented and discussed in this section.

3.3.1 Dynamic stability of a PWECB: cycle life

Prior to describing the dynamic stability of a PWECB using the K-PAMPS electrolyte, it is worthwhile to mention that using the

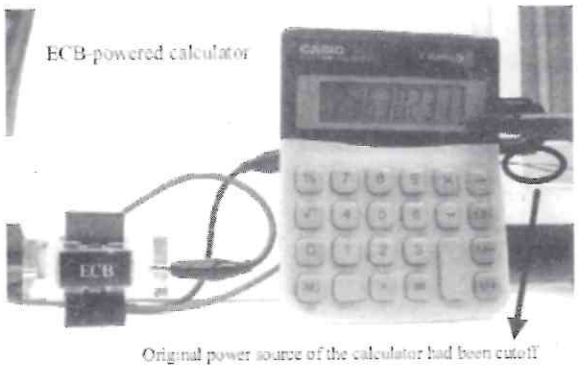

Figure 5: Demonstration of a PWECB-powered electronic calculator.

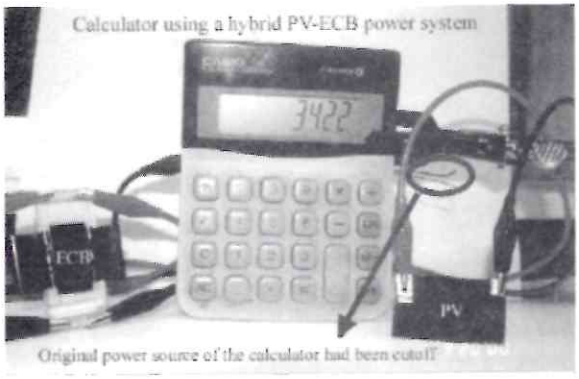

Figure 6: Demonstration of an all-solar-driven electronic calculator using the combinative PV-ECB power system.

K-PAMPS electrolyte has an advantage over the aqueous electrolyte as far as the cycle life of a PWECB is concerned. This is concluded from our earlier observations. Of course, this is because the SPE prevents the thicker EC films from peeling off the FTO substrates, as reported in literature [13-16]. For using the K-PAMPS electrolyte, Fig. 7 describes the cycling characteristics of a fresh PWECB, which was charged/discharged between 0.80V and 1.80V 1,000 times by applying a current density of 0.4 mA/cm^2. In this figure, two indices, η_n and θ_n, are defined and plotted to evaluate the dynamic stability: η_n denotes the ratio of the nth discharge capacity to the nth charge capacity, *i.e.*, the discharge-to-charge efficiency of the nth cycle; θ_n represents the discharge capacity ratio of the nth cycle to the 1^{st} cycle and can be viewed as a measure of the cycling loss in discharge capacity. It is shown that η_n, initially *ca.* 57%, increases rapidly in the first 10 cycles to a value of *ca.* 95% and then approaches 100% eventually. This implies that the fresh PWECB requires at least 10 cycles to attain a good discharge-to-charge efficiency. On the other hand, θ_n remains higher than *ca.* 97% in the first 100 cycles and then deceases gradually (0.062 % per cycle) to *ca.* 41% at the 1,000th cycle. Note that the cycle life of the PWECB is better than those reported in the PB-based secondary batteries [12-21]. Regarding the capacity-fading mechanism, the 100% discharge-to-charge efficiency (η_n) implies that the cycling loss in discharge capacity after 100 cycles is not attributed to electrochemical irreversibility. We suggest that the cycling loss is due to the formation of PY ($Fe[Fe(CN)_6]$), which decomposes and results in the formation of Fe^{3+} and $[Fe(CN)_6]^{3-}$, at a high cell voltage, such as 1.8V. This view is primarily supported by the two-electrode voltammogram of a PWECB (v = 10 mV/s), as shown in Fig. 8. As compared with Fig. 2, Fig. 8 reveals that the voltammogram after 100 voltammetric cycles is totally characterized by the BG/PB redox couple, whereas both PB and WO_3 dominate the 1^{st} cycle. This implies that it is PB rather than WO_3 that suffers from a capacity fading during the voltammetric cycling between 0.80V and 1.80V, because the two-electrode voltammogram is dominated by the electrode with a lower capacity [37]. Furthermore, a cycling loss in the cell's capacity of *ca.* 24% is observed in the 100-scan voltammogram. According to Fig. 7, an equivalent cycling loss of 24% recorded by chronopotentiometry is reached after the 450th cycle. It is inferred that cyclic voltammetry, which forces a PWECB to stay at high voltages for a longer time, is unfavorable for a cycle life test and causes a more serious capacity fading. In brief, lowering the upper boundary of the charging voltage and shortening the duration at unfavorably high voltages should improve the dynamic stability of a PWECB.

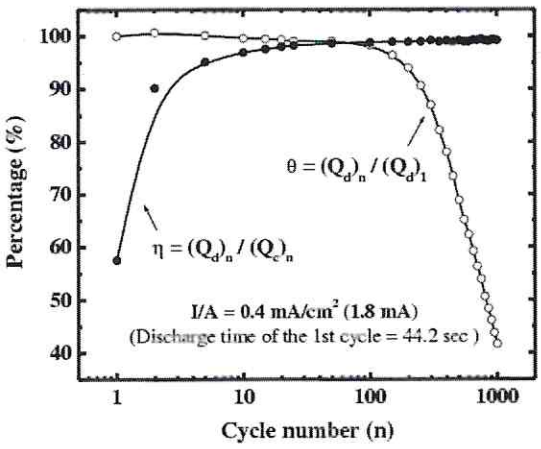

Figure 7: Cycling characteristics of a fresh PWECB, which was charged/discharged between 0.80V and 1.80V 1,000 times.

3.3.2 *At-rest stability of a PWECB: self-discharging rate*

To determine the at-rest stability of a PWECB, a self-discharging experiment was carried out, and the result is given on the left-hand side of Fig. 9. Prior to recording the open-circuit volt-

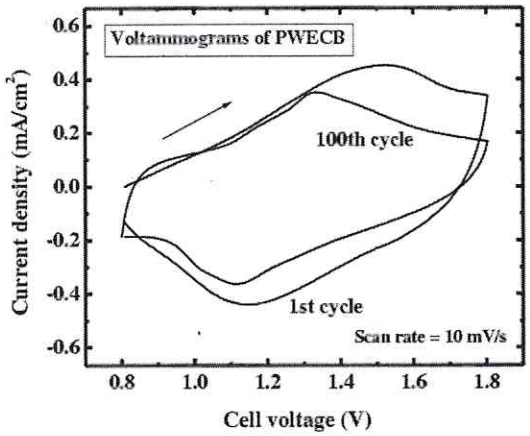

Figure 8: Comparison between the two-electrode voltammograms of the 1^{st} cycle and the 100^{th} cycle for a PWECB

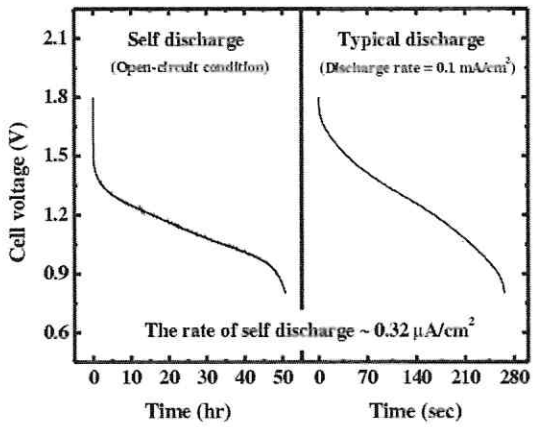

Figure 9: Comparison between self-discharging and typical discharging of a PWECB.

age during the self-discharging process, a PWECB was charged at a rate of 0.1 mA/cm^2 until arriving at 1.80V. Fig. 9 shows that it takes more than two days to self-discharge the fully charged PWECB to a cell voltage of 0.80V. When compared with typical discharging behavior, as shown on the right-hand side of Fig. 9, a small self-discharging rate of *ca.* 0.32 μA/cm^2 is estimated. This small self-discharging rate indicates that it will take *ca.* 3,125 hours (about 130 days) to self-discharge a PWECB with a capacity of 1 mAh/cm^2, if a good sealing condition is ensured! The applicability of a PWECB is thus further proven. Concerning the cause for the self-discharge of a fully charged PWECB (BG/K-PAMPS/$H_{1/3}WO_3$), presumably it is attributed to the presence of H_2O and O_2 in the K-PAMPS electrolyte, which will react with BG and $H_{1/3}WO_3$, respectively. The related mechanisms are suggested as follows:

$$\text{Positive electrode:} \quad BG + 1/3H_2O + 2/3K^+ \rightarrow PB + 1/6O_2 + 2/3H^+ \quad (4)$$

$$\text{Negative electrode:} \quad H_{1/3}WO_3 + 1/12O_2 \rightarrow WO_3 + 1/6H_2O \quad (5)$$

Reaction (4) describes the chemical reduction of BG in the presence of H_2O to form PB; reaction (5) elucidates the chemical oxidation of H_xWO_3 in the presence of oxygen. A similar self-bleaching (self-oxidizing) mechanism of H_xWO_3 was reported for a complementary PB-WO_3 ECD [9]. By considering the standard potential for the electro-hydrolysis process in the presence of H^+ [38] and the formal potentials for the BG/PB and WO_3/H_xWO_3 redox couples from Fig. 2, the standard Gibbs free energy (ΔG^o at 25°C) for the above two reactions are estimated to be 3.73 kJ/mole BG and -33.90 kJ/mole $H_{1/3}WO_3$, respectively. This indicates that the driving force of the self-discharging process for a PWECB is predominately contributed to by the spontaneous chemical oxidation of $H_{1/3}WO_3$ in the presence of oxygen. Thus, the above numbers can be used to explain why a self-discharging process, which discharges much more slowly, shows a lower cell voltage than that of a typical discharging process (see Fig. 9). To sum up, the amounts of the existing water and oxygen in the K-PAMPS electrolyte play a crucial role in determining the at-rest stability of a PWECB.

4. CONCLUSION

The applicability of a novel thin-film PWECB, which undergoes the BG/PB and WO_3/H_xWO_3 redox reactions and employs a K-PAMPS electrolyte to accommodate the conduction of both K^+ and H^+, has been demonstrated. In conclusion, some crucial findings on a PWECB are summarized as follows.

1. *High cell voltage*: A PWECB can be charged/discharged between 0.80 V and 1.80 V and provides a theoretical voltage of 1.35 V, which is almost twice the voltage of non-lithium PB-based secondary batteries and is even higher than that of a commercial Ni-MH battery.

2. *Visualization of the state of charge (SOC)*: A PWECB exhibits blue-to-dark green electrochromism during the charging process. Therefore, it offers visualization of the SOC.

3. *High electrochemical reversibility*: After 10 charge/discharge cycles, a discharge-to-charge efficiency of 95 % is

reached, and 100% efficiency is attained after 100 cycles and is kept for at least 900 more cycles. Although a fading rate in discharge capacity of *ca.* 0.06% per cycle is observed, it can be improved by shortening the duration at unfavorably high voltages to prevent the formation of degradable PY.

4. *Slow self-discharge*: The self-discharging rate is estimated to be as small as 0.32 μA/cm^2. In an ideal sealing situation, this means that it will take 130 days to self-discharge a PWECB with a capacity of 1 mAh/cm^2.

5. *Application in low-power electronic devices*: A thin-film PWECB with an energy capacity of *ca.* 37.8 mW-s/cm^2 is capable of driving an 8-digit electronic calculator for several hours.

6. *Superior storage for solar energy*: The combinative PV-ECB power system offers the opportunity to achieve an all-solar-driven low-power electronic device. The use of primary button batteries, which are harmful to the environment, can thus be eliminated.

Besides, a thin-film PWECB also has the advantages of easy production, low cost, and no leakage of electrolyte. Hence, we believe that the present work will stimulate the development of high-performance ECBs and provide a new choice in the use of batteries.

5. ACKNOWLEDGMENTS

The authors wish to thank Sinonar Corporation, Hsinchu, Taiwan, for providing the conductive FTO-coated glass substrates. This research was supported by the National Research Council of the Republic of China under Grant NSC 89-2214-E002-072.

REFERENCES

[1] P. M. S. Monk, R. J. Motimer, and D. R. Rosseinsky, *Electrochromism: Fundamentals and Applications*, VCH, Weinheim, Germany (1995).

[2] B. W. Faughnan, R. S. Crandall, and P. M. Heyman, *RCA Rev.*, **36**, 177 (1975).

[3] K. Itaya, K. Shibayama, H. Akahoshi, and S. Toshima, *J. Appl. Phys.*, 53, 804 (1982).

[4] F. G. K. Baucke, in "Proceedings of the International Society for Optical Engineering (SPIE)", "*Large-Area Chromogenics: Materials and Devices for Transmittance Control*", Eds., C. M. Lampert and C. G. Granqvist, Bellingham, 1990, **IS 4**, p. 518.

[5] R. D. Rauh, *Electrochim. Acta*, **44**, 3165 (1999).

[6] C. Bechinger, S. Ferrere, A. Zaban, J. Sprague, and B. Gregg, *Nature*, **383**, 608 (1996).

[7] M. Nishizawa, S. Kuwabata, and H. Yoneyama, *J. Electrochem. Soc.*, **143**, 3462 (1996).

[8] K.-C. Ho, T. G. Rukavina, and C. B. Greenberg, *J. Electrochem. Soc.*, **141**, 2061 (1994).

[9] K.-C. Ho, *Electrochim. Acta*, **44**, 3227 (1999).

[10] R. J. Mortimer and D. R. Rosseinsky, *J. Electroanal. Chem.*, **151**, 133 (1983).

[11] K. Itaya, I. Uchida, and V. D. Neff, *Acc. Chem. Res.*, **19**, 162 (1986).

[12] V. D. Neff, *J. Electrochem. Soc.*, **132**, 1382 (1985).

[13] K. Honda, J. Ochiai, and H. Hayashi, *J. Chem. Soc., Chem. Commun.*, 168 (1986).

[14] K. Honda and H. Hayashi, *J. Electrochem. Soc.*, **134**, 1330 (1987).

[15] M. Kaneko and T. Okada, *J. Electroanal. Chem.*, **255**, 45 (1988).

[16] M. Jayalakshimi and F. Scholz, *J. Power Sources*, **87**, 212 (2000).

[17] K. Kuwabara, J. Nunome, and K. Sugiyama, *J. Electrochem. Soc.*, **137**, 2001 (1990).

[18] K. Kuwabara, J. Itoh, and K. Sugiyama, *J. Mater. Sci.*, **27**, 5315 (1992).

[19] E. W. Grabner and S. Kalwellis-Mohn, *J. Appl. Electrochem.*, **17**, 653 (1987).

[20] M. Jayalakshmi and F. Scholz, *J. Power Sources*, **91**, 217 (2000).

[21] N. Imanishi, T. Morikawa, J. Kondo, Y. Takeda, O. Yamamoto, N. Kinugasa, and T. Yamagishi, *J. Power Sources*, **79**, 215 (2000).

[22] M. Broussely, P. Biensan, and B. Simon, *Electrochim. Acta*, **45**, 3 (1999).

[23] S. K. Deb, *Appl. Opt. Suppl.*, **3**, 193 (1969).

[24] R. S. Crandall, P. J. Wojtowicz, and B. W. Faughnan, *Solid State Commun.*, **18**, 1409 (1976).

[25] C. G. Granqvist, *Solar Energy Mater. & Solar Cells*, **60**, 201 (2000).

[26] J.-P. Randin, *J. Electrochem. Soc.*, **129**, 1215 (1982).

[27] R. D. Giglia, U. S. Pat., 4,375,318 (1983).

[28] T. Kase, M. Kawai, and M. Ura, *SAE Technical Paper Series*, 861,362 (1986).

[29] M. A. Habib, S. P. Maheswari, and M. K. Carpenter, *J. Appl. Electrochem.*, **21**, 203 (1991).

[30] H. Ohno and H. Yamazaki, *Solid State Ionics*, **59**, 217 (1993).

[31] K. Yamanaka, H. Oakamoto, H. Kidou, and T. Kudo, *Jap. J. Appl. Phys.*, **25**, 1420 (1986).

[32] L. H. Dao, A. Guerfi, and M. T. Nguyen, in "Proceedings of the Electrochemical Society", "*Electrochromic Materials*", Eds., M. K. Carpenter and D. A. Corrigan, Pennington, 1990, **PV90-2**, p.30.

[33] P. K. Shen, J. Syed-Bokhari, and A. C. C. Tseung, *J. Electrochem. Soc.*, **138**, 2778 (1991).

[34] I. Shiyanovskaya, M. Hepel, and E. Tewksburry, *J. New Mater. Electrochem. Systems*, **3**, 241 (2000).

[35] R. S. Crandall and B. W. Faughnan, *Phys. Rev. Lett.*, **39**, 232 (1977).

[36] J. B. Goodenough, *Prog. Solid State Chem.*, **5**, 315 (1971).

[37] L.-C. Chen and K.-C. Ho, *Electrochim. Acta*, **46**, 2159 (2001).

[38] A. J. Bard and L. R. Faulkner, *Electrochemical Methods: Fundamentals and Applications*, 2^{nd} ed., John Wiley & Sons, USA (2001): Table C.1 in Appendix C.